



A Quantum-Chemical Study of the Relationships between Electronic Structure and Anti-Proliferative Activities of Quinoxaline Derivatives on the K562 and MCF-7 Cell Lines

Gaston A. Kpotin^{1*}, Juan S. Gómez-Jeria²

¹Department of Chemistry, Faculty of Sciences and Technologies, University of Abomey-Calavi, Republic of Benin

²Quantum Pharmacology Unit, Department of Chemistry, Faculty of Sciences, University of Chile. Las Palmeras 3425, Santiago 7800003, Chile

Abstract We present here the results of a study of the relationship between electronic structure and anti-proliferative activities of quinoxaline derivatives on the K562 and MCF-7 cell lines. The Klopman-Peradejordi-Gómez method was employed. For each cell line we obtained a statistically significant equation relating the variation of the logarithm of IC₅₀ with the variation of the numerical values of a set of some local atomic reactivity indices. The process seems to be mainly orbital-controlled for the K562 cell line and orientational and orbital-controlled for the MCF-7 cell line. Based on the analysis of the results, a partial two-dimensional pharmacophore was built for each of the two cell lines. The results should be useful to propose new molecules with higher activity.

Keywords QSAR, quinoxaline, K562 cell, MCF-7 cell, pharmacophore

1. Introduction

Cancer is a large group of diseases that can reach any part of the body, and characterized by the rapid proliferation of abnormal cells. Cancer is the second leading cause of death globally, and was responsible for 8.8 million deaths in 2015. The most common causes of cancer death are cancers of lung, liver, colorectal, stomach and breast [1]. The modes of treatment of these diseases are surgery, radiotherapy and chemotherapy. Chemotherapy alone can be effective for a small number of cancers. It uses molecules that attack cancer cells inhibiting their growth. Chemotherapy sometimes causes adverse effects. But given its importance newer and more effective molecules are constantly being synthesized and tested [2–21].

Some specific cell lines were used for *in vivo* or *in vitro* studies. MCF-7, acronym of Michigan Cancer Foundation-7, is the cell line most used for breast cancer studies [22]. K562 cells were the first human immortalized myelogenous leukemia line to be established. K562 cells are of the erythroleukemia type, and the line is derived from a 53-year-old female chronic myelogenous leukemia patient in blast crisis [23]. Some quinoxaline has antiproliferative activity on K562 and MCF-7 cell lines. (±)-2-[4-(7-chloro-2-quinoxalinyloxy)phenoxy]propionic acid is an important lead compound against a broad spectrum of solid tumors. It has high activity for numerous types of multidrug resistance (MDR) cancers [6]. Because of the asymmetric carbon substituted by R₄ we have two isomers, the R(+) and the S(-). The R(+) stereoisomer is slightly more potent than S(-)-isomer [24]. The antiproliferative activity mechanism is not clearly known, but some attempts of mechanisms were proposed [25–32]. The study of the structure-activity relationships (SAR) is important for the synthesis of new and more active molecules. There are several statistics-based SAR methods for carrying out such task. On the side of the model-based methods, the Klopman-Peradejordi-Gómez (KPG) approach has proven to be very useful to disclose the



relationships between electronic structure and receptor affinity. Recently, it was shown that, for a group of molecules having a complex biological activity expressed through the same many-step mechanism, the KPG method could also be used with excellent results. The use of the KPG method relating antiproliferative activity and electronic structure for several group of different molecules were effective[33–37].

In this paper we present the results of a quantum-chemical analysis of the relationships between the electronic structure and the antiproliferative activity against the K562 and MCF-7 cell lines of a series of quinoxaline derivatives. From the results obtained we propose the associated two-dimensional (2D) antiproliferative partial pharmacophores.

2. Methods, Models and Calculations

2.1. Model and Selection of Molecules

Since the KPG method has been extensively discussed in many previous papers, we present here only a short summary [38]. As we said before, this method was originally developed for the study of drug-receptor equilibrium constants (pA_2 , K_i , IC_{50}). Considering that many of the *in vitro* effects are the ultimate result of two or more unidentified or unsatisfactorily known processes, that all these processes can be described in terms of the electronic structure of the molecules and that this electronic structure is described by the same reactivity indices describing equilibrium constants, a preliminary representation of the final biological action can be obtained simply by replacing $\log K_i$ by $\log (BA)$, where BA is any biological *in vitro* or *in vivo* activity.

Therefore, the antiproliferative activity, AA, can be expressed as a linear relationship of the form:

$$\log(AA) = a + \sum_j [e_j Q_j + f_j S_j^E + s_j S_j^N] + \sum_j \sum_m [h_j(m) F_j(m) + x_j(m) S_j^E(m)] + \sum_j \sum_m [r_j(m') F_j(m') + t_j(m') S_j^N(m')] + \sum_j [g_j \mu_j + k_j \eta_j + o_j \omega_j + z_j \zeta_j + w_j Q_j^{\max}] + \sum_{k=1}^U O_k \quad (1)$$

where Q_j is the net charge of atom j , S_j^E and S_j^N are, respectively, the total atomic electrophilic and nucleophilic superdelocalizabilities of atom j , $F_{j,m}(F_{j,m'})$ is the Fukui index of the occupied (vacant) MO $m(m')$ located on atom j [39]. $S_j^E(m)$ is the atomic electrophilic superdelocalizability of MO m on atom j , etc. The total atomic electrophilic superdelocalizability of atom j corresponds to the sum over occupied MOs of the $S_j^E(m)$'s and the total atomic nucleophilic superdelocalizability of atom j is the sum over vacant MOs of $S_j^N(m)$'s[40]. μ_j is the local atomic electronic chemical potential of atom j , η_j is the local atomic hardness of atom j , ω_j is the local atomic electrophilicity of atom j , ζ_j is the local atomic softness of atom j , and Q_j^{\max} is the maximum amount of electronic charge that atom j may accept from another site[40]. O_k 's are the orientational parameters of the substituents [41]. Throughout this paper $HOMO_j^*$ refers to the highest occupied molecular orbital localized on atom j and $LUMO_j^*$ to the lowest empty MO localized on atom j . They are called the local atomic frontier MOs.

The application this model has given excellent results for a great variety of drug-receptor systems and biological activities [33–37, 42–50]. Therefore, for each molecule of the group studied we have one Eq. 1. Usually enough experimental data to solve the linear system of equations 1 cannot be found in the literature. This force us to use linear multiple regression techniques in order to find those reactivity indices whose numerical variation gives an account of the variation of the antiproliferative activity.

The structures of the compounds are shown in Figure 1 (R_4 is behind the plane) and Table 1 summarizes the values of their median inhibitory concentrations expressed as $\log(IC_{50})$ for the R(+)-isomer [6].



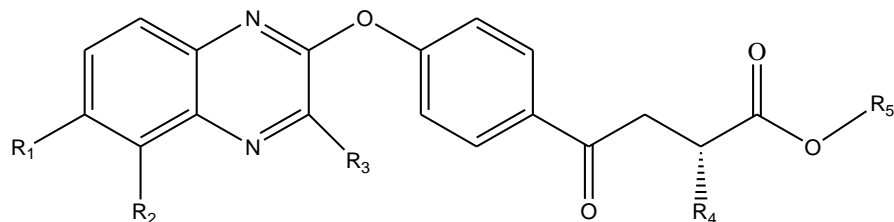


Figure 1: Structure of quinoxaline derivatives

Table 1: Quinoxalines and their experimental anti-proliferative activity

Mol.	R ₁	R ₂	R ₃	R ₄	R ₅	log(IC ₅₀)MCF-7	log(IC ₅₀)K562
1	H	H	CH ₃	CH ₃	CH ₃	1.58	1.66
2	H	H	CH ₃	(CH ₃) ₂ CHCH ₂ -	CH ₃	1.41	1.35
3	H	H	CH ₃	CH ₃ CH ₂ CH(CH ₃)-	CH ₃	1.56	1.58
4	H	Cl	CH ₃	CH ₃	CH ₃	1.53	1.42
5	H	Cl	CH ₃	(CH ₃) ₂ CHCH ₂ -	CH ₃	1.36	1.51
6	Cl	H	CH ₃	C ₆ H ₅ CH ₂ -	CH ₃	1.41	1.44
7	Cl	H	CH ₃	(CH ₃) ₂ CHCH ₂ -	CH ₃	1.28	1.34
8	H	H	CH ₃	CH ₃	H	1.41	1.45
9	H	H	CH ₃	(CH ₃) ₂ CHCH ₂ -	H	1.17	1.29
10	H	H	CH ₃	CH ₃ CH ₂ CH(CH ₃)-	H	1.55	1.48
11	H	Cl	CH ₃	CH ₃	H	1.29	1.32
12	H	Cl	CH ₃	(CH ₃) ₂ CHCH ₂ -	H	1.24	1.33
13	Cl	H	CH ₃	C ₆ H ₅ CH ₂ -	H	1.30	1.33
14	Cl	H	CH ₃	(CH ₃) ₂ CHCH ₂ -	H	1.18	1.16
15	H	H	NH(CH ₂) ₁₁ CH ₃	C ₆ H ₅ CH ₂ -	CH ₃	1.52	1.48
16	H	H	NH(CH ₂) ₁₁ CH ₃	CH ₃	CH ₃	1.53	1.43
17	H	H	NH(CH ₂) ₁₁ CH ₃	(CH ₃) ₂ CHCH ₂ -	CH ₃	1.64	1.49
18	H	H	NH(CH ₂) ₁₁ CH ₃	H	CH ₃	1.58	1.63
19	H	H	NHC(CH ₂) ₃	CH ₃	CH ₃	1.52	1.59
20	H	H	NHC(CH ₂) ₃	C ₆ H ₅ CH ₂ -	CH ₃	---	1.01
21	H	H	NH(CH ₂) ₁₁ CH ₃	C ₆ H ₅ CH ₂ -	H	0.83	0.87
22	H	H	NH(CH ₂) ₁₁ CH ₃	CH ₃	H	0.61	0.52
23	H	H	NH(CH ₂) ₁₁ CH ₃	(CH ₃) ₂ CHCH ₂ -	H	1.48	1.33
24	H	H	NH(CH ₂) ₁₁ CH ₃	H	H	1.47	1.42
25	H	H	NHC(CH ₂) ₃	CH ₃	H	1.05	1.26
26	H	H	NHC(CH ₂) ₃	CH ₃ CH ₂ CH(CH ₃)-	H	1.61	1.63
27	H	H	NHC(CH ₂) ₃	C ₆ H ₅ CH ₂ -	H	1.40	1.18

2.2. Calculations

The Gaussian03 package of software [51] was used to optimize the geometry of all molecules in their neutral form. The calculations were performed within the Density Functional Theory (DFT) at the B3LYP/6-31G(d,p) level. The D-Cent-QSAR software [52] was used to calculate the local atomic reactivity indices from the single point results of Gaussian03. All electron populations lesser than or equal to 0.01e are considered null [53]. The orientational parameters of the substituents are calculated in the usual manner [54]. We used the concept of common skeleton defined as a set of atoms common to all the molecules analyzed. We hypothesize that the variation of the numerical values of the local atomic reactivity indices (LARIs) of the atoms of this common skeleton accounts for almost all the variation of the biological activity. The numbering of the atoms of the common is shown in Fig. 2.



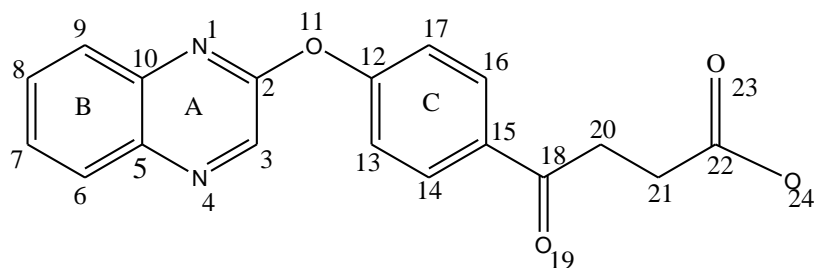


Figure 2: Common skeleton numbering

For linear multiple regression analysis (LMRA) a data matrix containing $\log(IC_{50})$ as the dependent variable and the local atomic reactivity indices of all the atoms of the common skeleton as independent variables was used. The Statistica software was used to perform LMRA studies[55].

3. Results

3.1 Results for the anti-proliferation activities on K562 cells.

The best statistically significant equation obtained is the following:

$$\log(IC_{50}) = -20.19 - 2.32S_{21}^E + 1.66F_{21}(HOMO)^* - 5.13F_{13}(LUMO)^* + 3.15F_{18}(LUMO)^* + 0.16F_{19}(HOMO)^* + 0.49F_6(LUMO)^* + 0.66S_{23}^E(HOMO)^* \quad (2)$$

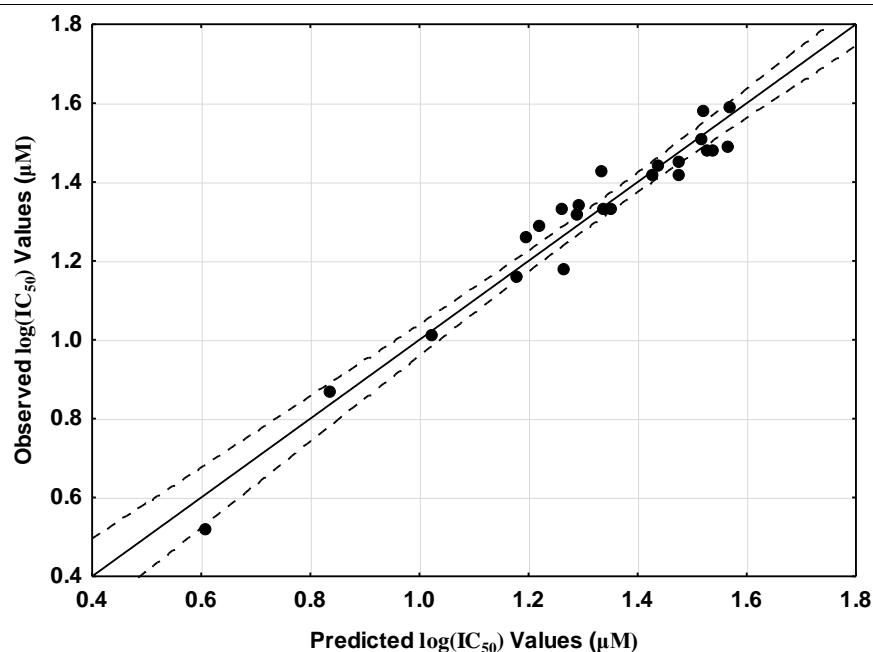
with $n=23$, $R=0.97$, $R^2=0.95$, $\text{adj-}R^2=0.93$, $F(7,15)=42.63$ ($p < 0.000001$) and a standard error of estimate of 0.06. No outliers were detected and no residuals fall outside the $\pm 2\sigma$ limits. Here S_{21}^E is the total atomic electrophilic superdelocalizability of atom 21, $F_{21}(HOMO)^*$ is the electron population (Fukui index) of the highest occupied MO localized on atom 21, $F_{13}(LUMO)^*$ is the electron population of the lowest empty MO localized on atom 13, $F_{18}(LUMO)^*$ is the electron population of the lowest empty MO localized on atom 11, $F_{19}(HOMO)^*$ is the electron population of the highest occupied MO localized on atom 19, $F_6(LUMO)^*$ is the electron population of the lowest empty MO localized on atom 4, $S_{23}^E(HOMO)^*$ is the atomic electrophilic superdelocalizability of the third lowest empty MO localized on atom 23. Table 2 shows the beta coefficients and the t-test results for the significance of coefficients of equation 2. Concerning independent variables, Table 3 shows that there are no significant correlations among the reactivity indices. Fig. 3 shows the plot of observed vs. calculated values of $\log(IC_{50})$. The associated statistical parameters of Eq. 2 show that this equation is statistically significant and that the variation of the numerical values of seven LARIs explains about 93% of the variation of the biological activity.

Table 2: Beta coefficients and t-test for significance of coefficients in equation 2

Variable	Beta coefficients	t(15)	p-Value
S_{21}^E	-0.87	-12.82	0.0000001
$F_{21}(HOMO)^*$	0.56	8.58	0.0000001
$F_{13}(LUMO)^*$	-0.80	-11.11	0.0000001
$F_{18}(LUMO)^*$	0.42	6.71	0.0000007
$F_{19}(HOMO)^*$	0.35	5.08	0.0001
$F_6(LUMO)^*$	0.26	4.16	0.0008
$S_{23}^E(HOMO)^*$	0.15	2.32	0.03

Table 3: Squared correlation coefficients for the variables appearing in Eq.2

	S_{21}^E	$F_{21}(HOMO)^*$	$F_{13}(LUMO)^*$	$F_{18}(LUMO)^*$	$F_{19}(HOMO)^*$	$F_6(LUMO)^*$
$F_{21}(HOMO)^*$	0.02					
$F_{13}(LUMO)^*$	0.12	0.01				
$F_{18}(LUMO)^*$	0.00	0.01	0.14			
$F_{19}(HOMO)^*$	0.09	0.08	0.06	0.02		
$F_6(LUMO)^*$	0.02	0.002	0.005	0.006	0.05	
$S_{23}^E(HOMO)^*$	0.02	0.20	0.002	0.002	0.02	0.08

Figure 3: Plot of predicted vs. observed $\log(IC_{50})$ values. Dashed lines denote the 95% confidence interval

3.2. Results for the anti-proliferation activities on MCF-7 cells

The best statistically significant equation obtained is the following:

$$\log(IC_{50}) = 2.96 - 0.90S_1^E(HOMO)^* - 0.002\varphi_{R_2} + 0.69\mu_{22} - 0.40F_6(HOMO)^* - 1.84F_{22}(HOMO)^* + 2.67\zeta_{16} \quad (3)$$

with $n=22$, $R=0.98$, $R^2=0.95$, $\text{adj-}R^2=0.94$, $F(6,15)=51.70$ ($p < 0.000001$) and a standard error of estimate of 0.05.

No outliers were detected and no residuals fall outside the $\pm 2\sigma$ limits. Here $S_1^E(HOMO)^*$ is the atomic electrophilic superdelocalizability of highest occupied MO localized on atom 15, φ_{R_2} is the orientational parameter (OP) of the R_2 substituent, μ_{22} is the local atomic electronic chemical potential of atom 22, $F_6(HOMO)^*$ is the electron population of the highest occupied MO localized on atom 6, $F_{22}(HOMO)^*$ is the electron population of the highest occupied MO localized on atom 22 and ζ_{16} is the local atomic softness of atom 16.



Table 4 shows the beta coefficients and the t-test results for the significance of coefficients of equation 3. Concerning independent variables, Table V shows that the highest internal correlation is $r^2 (F_6(HOMO))^*$, $S_1^E(HOMO)^*)=0.40$. Fig. 4 shows the plot of observed values vs. calculated values of $\log(IC_{50})$. The associated statistical parameters of Eq. 3 show that this equation is statistically significant and that the variation of the numerical values of six LARIs explains about 94% of the variation of the biological activity.

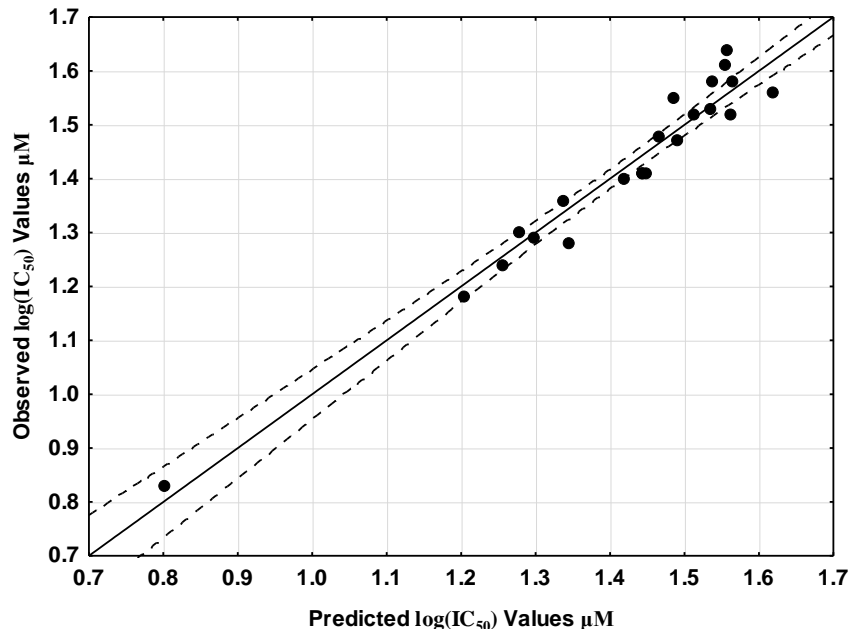


Figure 4: Plot of predicted vs. observed $\log(IC_{50})$ values. Dashed lines denote the 95% confidence interval

Table 4: Beta coefficients and t-test for significance of coefficients in equation 3

Variable	Beta coefficients	t(15)	p-Value
$S_1^E(HOMO)^*$	-0.66	-8.80	0.000000
φ_{R2}	-0.38	-5.40	0.00007
μ_{22}	0.32	4.08	0.001
$F_6(HOMO)^*$	-0.22	-2.93	0.01
$F_{22}(HOMO)^*$	-0.18	-2.46	0.03
ζ_{16}	0.16	2.32	0.03

Table 5: Squared correlation coefficients for the variables appearing in equation 3

	$S_1^E(HOMO)^*$	φ_{R2}	μ_{22}	$F_6(HOMO)^*$	$F_{22}(HOMO)^*$
φ_{R2}	0.02				
μ_{22}	0.10	0.02			
$F_6(HOMO)^*$	0.40	0.04	0.10		
$F_{22}(HOMO)^*$	0.03	0.05	0.32	0.10	
ζ_{16}	0.00	0.24	0.02	0.05	0.13

3.3. Local molecular orbitals

Tables VI and VII show the Local Molecular Orbitals of atom 1, 6, 13, 18, 19 and 21 (see Fig. 3). Nomenclature: Molecule (HOMO) / (HOMO-2)* (HOMO-1)* (HOMO)* - (LUMO)* (LUMO+1)* (LUMO+2)*.

Table 6: Local Molecular Orbitals of atoms 1, 6 and 13

Mol	Atom 1 (N)	Atom 6(C)	Atom 13 (C)
1(96)	94lp95π96π-97lp98lp99π	93π95π96π-97π98π99π	92π93π96π-97π98π100π
2 (108)	106lp107π108π-109π110lp111π	105σ107π108π-109π110π111π	104π105π108π-109π110π111π
3 (116)	113lp115lp116π-117lp118lp119π	113π115π116π-117π118π119π	113π115π116π-117π118π120π
4 (104)	101lp103lp104π-105lp106lp107π	101σ103π104π-105π106π107π	101π103π104π-105π106π108π
5 (116)	113lp115lp116π-117lp118lp119π	113σ115π116π-117π118π119π	113π115π116π-117π118π120π
6 (124)	120lp121π122π-125lp126lp127π	120π121π122π-125π126π127π	118π121π122π-125π126π128π
7 (116)	113lp114π116π-117lp118lp119π	113π114π116π-117π118π119π	112π114π116π-117π118π119π
8 (92)	90lp91π92π-93lp94lp95π	89σ91π92π-93π94π95π	88π89π92π-93π94π95π
9 (104)	102lp103π104π-105lp106lp107π	101σ103π104π-105π106π107π	100π101π104π-105π106π107π
10 (104)	102lp103π104π-105lp106lp107π	101σ103π104π-105π106π107π	100π101π104π-105π106π108π
11 (100)	97lp99lp100π-101lp102lp103π	97σ99π100π-101π102π103π	97π99π100π-101π102π104π
12 (112)	109lp111lp112π-113lp114lp115π	109σ111π112π-113π114π115π	109π111π112π-113π114π116π
13 (120)	116lp117π118π-121lp122lp123π	115σ117π118π-121π122π123π	114π117π118π-121π122π124π
14 (112)	109lp110π112π-113lp114lp115π	110π111π112π-113π114π115π	108π110π112π-113π114π116π
15 (164)	158lp160lp162π-165lp166lp172lp	160σ162π164π-165π166π168π	158π159π162π-165π167π172π
16 (144)	140lp142lp143π-145lp146lp150π	142σ143π144π-145π146π148π	139π140π143π-145π147π150π
17 (156)	153lp15lp4155π-157lp158lp162lp	154σ155π156π-157π158π160π	151π152π155π-157π159π162π
18 (140)	136lp138lp139π-141lp142lp146lp	138π139π140π-141π142π144π	135π136π139π-141π143π146π
19 (112)	108lp109lp111π-113lp114lp118lp	109π111π112π-113π114π116π	107π108π111π-113π115π118π
20 (136)	131lp132lp134π-137lp138lp143lp	132π134π136π-137π138π140π	129π130π134π-137π139π144π
21 (160)	156lp158π159π-161lp162lp168	158π159π160π-161π162π164π	154π155π158π-161π163π168π
22 (140)	136lp138lp139π-141lp142lp146lp	138π139π140π-141π142π144π	135π136π139π-141π143π146π
23 (152)	148lp150lp151π-153lp154lp158	150π151π152π-153π154π156π	147π148π151π-153π155π158π
24 (136)	132lp134lp135π-137lp138lp142lp	134π135π136π-137π138π140π	131π132π135π-137π139π142π
25 (108)	104lp106lp107π-109lp110lp114lp	106π107π108π-109π110π112π	103π104π107π-109π111π114π
26 (120)	116lp118lp119π-121lp122lp126lp	118π119π120π-121π122π124π	115π116π119π-121π123π126π
27 (128)	122lp124lp126π-129lp130lp136lp	124π126π128π-129π130π132π	122π123π126π-129π131π136π

Table 7: Local Molecular Orbitals of atoms 18, 19, 21 and 22

Mol.	Atom 18 (C)	Atom 19 (O)	Atom 21 (C)	Atom 22 (C)
1(96)	86π87π94π- 97π98π99π	93lp94π96lp- 97lp98lp99π	86σ90σ94σ- 102σ105σ110σ	86π89π90π- 102π103π105π
2 (108)	93π94π106π- 109π110π111π	93π94π106lp- 109lp110lp111π	102σ103σ106σ- 114σ120σ124σ	94σ101π102π- 113π114π115π
3 (116)	102π107π114π- 117π118π119π	114π115lp116lp- 117lp118lp119π	111σ112σ114σ- 122σ129σ130σ	109π111π112π- 122π124σ126σ
4 (104)	92π93π102π- 105π106π107π	102π103lp104lp- 105lp106lp107π	93σ98σ102σ- 110σ114σ119σ	93σ97π98π- 110π112π114σ
5 (116)	100π102π114π- 117π118π119π	114π115lp116lp- 117lp118lp119π	107σ111σ114σ- 122σ128σ133σ	102σ109π111π- 122π124π126σ
6 (124)	106π107π120π- 125π126π127π	120π121lp122lp- 125lp126lp127π	117σ120σ124σ- 130σ131σ132σ	115π117π120σ- 130π131π132π
7 (116)	100π101π115π- 117π118π119π	114lp115π116lp- 117lp118lp119π	108σ111σ115σ- 122σ128σ133σ	101σ109π111π- 122π124π126σ
8 (92)	80π81π90π- 93π94π95π	89lp90π92lp- 93lp94lp95π	81σ86σ90σ- 97σ98σ100σ	81σ84π86π- 97π98π99π
9 (104)	90π93π102π- 105π106π107π	101lp102π104lp- 105lp106lp107π	97σ98σ102σ- 109σ110σ114σ	96π97π98π- 109π110π111π
10	90π93π102π- 105π106π107π	101lp102π104lp- 105lp106lp107π	97σ98σ102σ- 109σ110σ114σ	94π97π98π- 109π110π111π



(104)	105π106π107π	105lp106lp107π	110σ112σ114σ	109π110π112σ
11	88π89π98π-	98π99lp100lp-	89σ94σ98σ-	89σ91π94π-
(100)	101π102π103π	101lp102lp103π	106σ110σ111σ	106π108π110σ
12	95π97π110π-	110π111lp112lp-	104σ106σ110σ-	99π104π106π-
(112)	113π114π115π	113lp114lp115π	118σ123σ124σ	118π120π121σ
13	102π103σ116π-	116π117lp118lp-	112σ116σ120σ-	107π110π112π-
(120)	121π122π123π	121lp122lp123π	126σ127σ128σ	126π127π128π
14	96π97π111π-	110lp111π112lp-	105σ106σ111σ-	104105106-
(112)	113π114π115π	113lp114lp115π	118σ123σ124σ	118π120π122σ
15	138π158σ159π-	159π160lp162lp-	156σ159σ163σ-	141σ153π156π-
(164)	165π166π168π	165lp166lp172π	169σ170σ171σ	169π170π171π
16	123π125π141π-	141π142lp143lp-	125σ138σ141σ-	125σ135π138π-
(144)	145π146π148π	145lp146lp151lp	149σ165σ167σ	149π151π155
17	133π153π154π-	153π154π155lp-	145σ150σ151σ-	132π147π150π-
(156)	157π158π160π	157lp158lp163π	161σ172σ180σ	161π163π165
18	118π119π137π-	137π138lp139lp-	119σ134σ137σ-	119π131π134π-
(140)	141π142π144	141lp142lp147π	145σ149σ159σ	145π147π154σ
19	98σ99π110π-	109lp110π111lp-	99σ106σ110σ-	99π104π106π-
(112)	113π114π116π	113lp114lp119lp	117σ127σ128σ	117π119π121σ
20	130π131π132π-	131π132π134lp-	128σ132σ135σ-	121σ126128π-
(136)	137π138π140π	137lp138lp145π	141σ142σ143σ	141π142π143π
21	134π154π155π-	155π156lp158lp-	154σ155σ159σ-	143π148152-
(160)	161π162π164π	161lp162lp168π	165σ166σ167σ	165π166π167π
22	119π120π137π-	137π138lp139lp-	120σ134σ137σ-	128π129π134π-
(140)	141π142π144π	141lp142lp147π	145σ148σ150σ	145π147π148σ
23	127π128π149π-	149π150lp151lp-	142σ146σ149σ-	135π142π146π-
(152)	153π154π156π	153lp154lp159lp	157σ162σ166σ	157π159π160π
24	112π115π133π-	133π134lp135lp-	115σ130σ133σ-	106σ123π130π-
(136)	137π138π140π	137lp138lp143π	141σ146σ162σ	141π143π144π
25	94π95π105π-	105π106lp107lp-	95σ102σ105σ-	95σ99π102π-
(108)	109π110π112π	109lp110lp115π	113σ117σ118σ	113π115π117σ
26	109π116π117π-	117π118lp119lp-	111σ114σ117σ-	110π111π114π-
(120)	121π122π124π	121lp122lp127π	125σ129σ130σ	125π127σ129σ
27	110π122π123π-	123π124lp126lp-	120σ123σ127σ-	115π117π120π-
(128)	129π130π132π	129lp130lp137lp	133σ134σ135σ	133π134π135π

Figures 5 and 6 show the local (HOMO)* of atom 19. In the first case we observe clearly the lone pair orbital and in the second case we notice also the lone pair orbital with the big lobes which look like π MO. In the two cases the lobes are below and above the atom that is normal in carbonyl group.

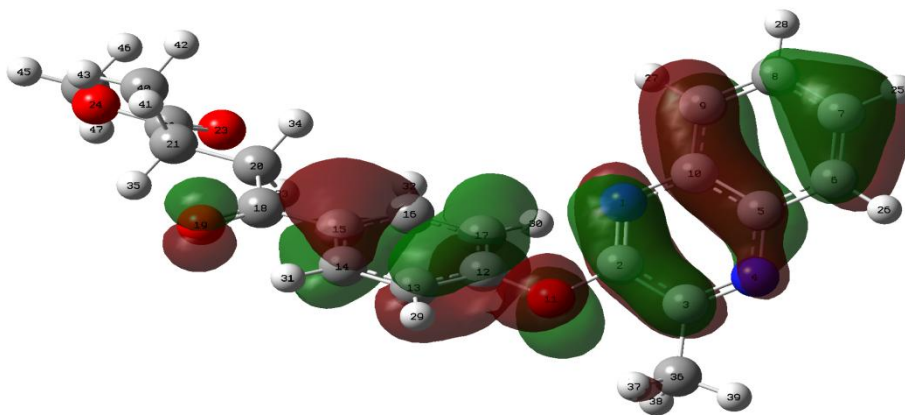


Figure 5: Local (HOMO)* of atom 19 of molecule1 (corresponding to the molecule's HOMO)

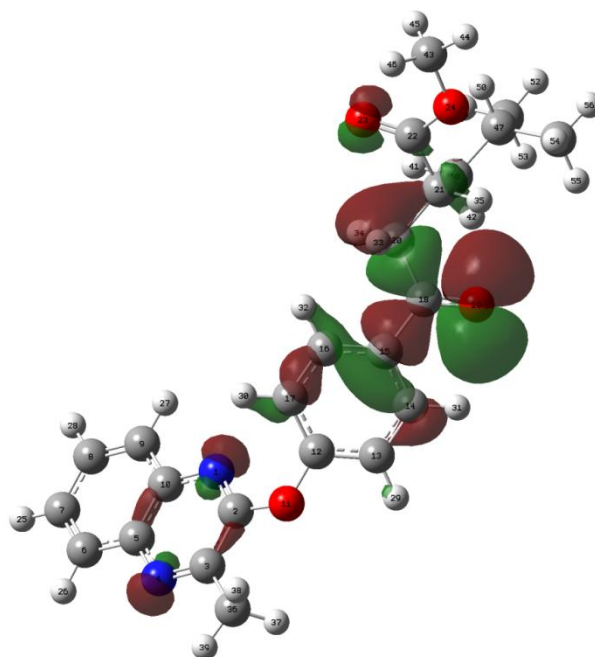


Fig 6: Local (HOMO)* of atom 19 of molecule2 (corresponding to the molecule's (HOMO-2)).

4. Discussion

Before discussing the equations we must stress that they contain only those terms related to the variation of IC_{50} through the series. We shall employ the variable by variable approach for the discussion (VbV). Also, it is important to understand that the binding pharmacophore is conceptually clear because it corresponds to a drug-receptor interaction. The inhibition pharmacophore is not.

4.1. Discussion for the anti-proliferation activities on K562 cells

The beta values shows that the importance of variables is $S_{21}^E > F_{13}(LUMO)^* > F_{21}(HOMO)^* > F_{18}(LUMO)^* > F_{19}(HOMO)^* > F_6(LUMO)^* > S_{23}^E(HOMO)^*$. The associated p-value of Table 2 indicates that $S_{23}^E(HOMO)^*$ is not significant, so we will only discuss the six others indices. The process seems to be orbital-controlled because all the indices depend on the electron population or/and the energies of the MOs. Keeping in mind that the values of the electrophilic superdelocalizability are always negative and the values of the Fukui index are always positive, aVbV analysis indicates that a good activity is associated with low negative numerical values of S_{21}^E , low positive numerical values for $F_{21}(HOMO)^*$, $F_{18}(LUMO)^*$, $F_{19}(HOMO)^*$, and $F_6(LUMO)^*$ and high numerical values for $F_{13}(LUMO)^*$. Atom 21 is the carbon atom of one of the CH_2 groups of the lateral chain of ring C (Fig. 2). All the local MOs of atom 21 are σ type. $HOMO_{21}^*$ does not coincide with the HOMO of the molecule (Table 7). Note that $(LUMO)_{21}^*$ is energetically far from the molecular LUMO. A low value of S_{21}^E indicates that atom 21 should behave as a bad electron donor. Eq. 2 indicates coincidentally also that a high activity is associated with a low numerical value of $F_{21}(HOMO)^*$. This suggests that atom 21 seems to be involved in a repulsive MO-MO interaction with one or more occupied MOs of the site. If these interactions are of the σ - σ kind, they may occur with the sigma MOs of the $-CH_2-$ groups of some amino acids. Atom 18 is the carbon atom of the



carbonyl group (Fig. 2). The association of high activity with low numerical values of $F_{18}(LUMO)^*$ suggests that this MO is engaged in a repulsive MO-MO interaction with empty MOs of the site. As $(LUMO)_{18}^*$ is a MO of π nature in all molecules and it coincides with the molecule's LUMO (Table 7), a better activity will be achieved if the molecular LUMO and next empty MOs are not localized on this atom. Atom 19 is the oxygen atom of the carbonyl group (Fig. 2). $(HOMO)_{19}^*$ is a lone pair (Table 7) in which the lobes are below and above the atom (fig.5,6). The low numerical value of $F_{19}(HOMO)^*$ suggests a repulsive MO-MO interaction with occupied MOs of the site. Therefore, activity will be higher if $(HOMO)_{19}^*$ corresponds to an occupied MO energetically far from the molecular HOMO. Atom 6 is a carbon atom of the aromatic ring A (Fig. 2). A high activity is associated with low numerical values of $F_6(LUMO)^*$. All the local LUMO* are of π nature (Table 6). Again we are in presence of what seems to be a repulsive MO-MO interaction. So an electro-deficient moiety could be substituted on atom 6. Atom 13 is a carbon atom of the aromatic ring C. $(LUMO)_{13}^*$ is a π MO in all molecules (Table 6). A high value for $F_{13}(LUMO)^*$ is associated with high inhibitory activity. Therefore, we suggest that atom 13 is interacting with a π electron-rich center. All these suggestions are presented in the partial 2D inhibition pharmacophore of Fig. 7.

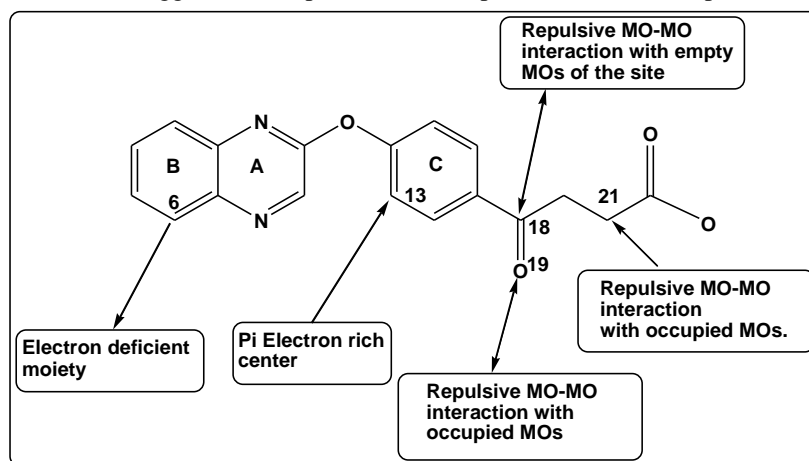


Figure 7: Partial 2D pharmacophore for the anti-proliferative activities of quinoxaline derivatives on the K562 cell line

4.2. Discussion for the anti-proliferative activities on MCF-7 cells

The beta values shows that the importance of variables is $S_1^E(HOMO)^* > \varphi_{R2} > \mu_{22} > F_6(HOMO)^* > F_{22}(HOMO)^* > \zeta_{16}$. The associate dp-values indicate that the last three indices are not significant, so we shall discuss the first three ones. The process seems to be orientational- and orbital-controlled. A VbV analysis indicates that a good activity is associated with low negative numerical values of $S_1^E(HOMO)^*$, a high value of φ_{R2} and high negative values of μ_{22} . Atom 1 is a nitrogen atom of the ring B (Fig.2). The local HOMO* of atom 1 is of π nature for all molecules (Table 4). $LUMO_1^*$ has a lone pair nature and it coincides with the molecular LUMO. The low numerical value of $S_1^E(HOMO)^*$ indicates that atom acts as a bad donor, so this atom should interact with an electron rich center of the receptor, possibly a π - π interaction. R_2 is the substituent on atom 6. The high value of φ_{R2} suggests that R_2 should be a big substituent or that the substituent must be in its extended form. Atom 22 is a carbon atom of the carboxylate group. A higher negative value of μ_{22} should be obtained by making more negative the HOMO* energy, making this atom a bad electron donor. Note that this atom is a bad electron-donor because its local $HOMO_{22}^*$ is energetically far for the molecule's HOMO (Table 7). Theoretically we may lower the value of

μ_{22} by making zero the electron population of the actual HOMO_{22}^* , i.e., changing it by a still energetically lower MO. But Table 7 informs us that, given the nature of the actual $(\text{HOMO})_{22}^*$, this technique will be very difficult to use. Now, Table 7 shows that $(\text{LUMO})_{22}^*$ does not coincide with the molecular LUMO. Therefore another possibility is to localize the molecular HOMO also on atom 22. This technique seems more plausible because atom 22 has a positive net charge. Therefore, atom 22 seems to interact with an electron rich center of a probable π nature. All these suggestions are presented in the partial 2D inhibition pharmacophore of Fig. 8.

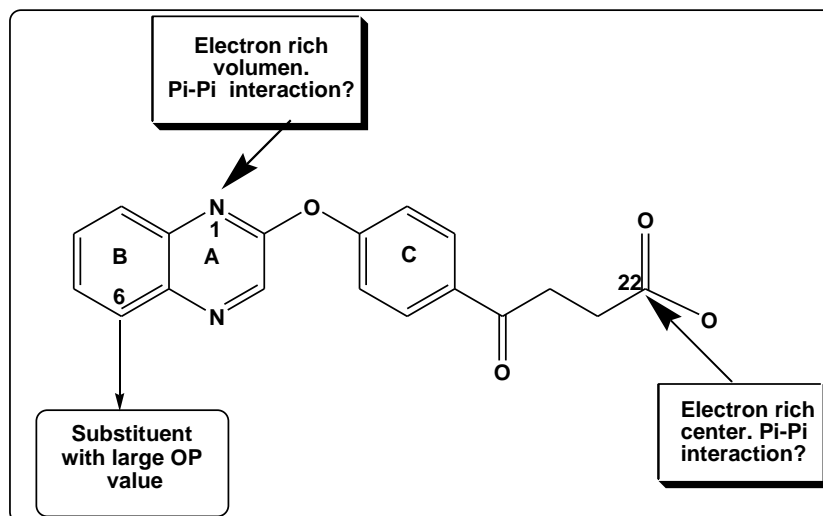


Figure 8: Partial 2D pharmacophore for the anti-proliferative activities of quinoxaline derivatives on the MCF-7 cell line

5. Conclusion

In summary, we have obtained a statistically significant equations which can be used to predict the antiproliferative activity of quinoxaline derivative on K562 and MCF-7 cell lines. The obtained pharmacophores show the chemical modification that are useful to propose some molecules which will be more actives.

References

1. Cancer. <http://www.who.int/news-room/fact-sheets/detail/cancer>, 1st february 2018
2. Zhen, X., Fei, L., Xiuying, C., Xiaolei, W., Lujie, C., Kejun, Y., Wufu, Z. and Shan, X. Design, synthesis, and antitumor evaluation of quinoline-imidazole derivatives. Arch. Pharm. (Weinheim) 0, e1700407.
3. Banu, S., Bollu, R., Bantu, R., Nagarapu, L., Polepalli, S., Jain, N., Vangala, R. and Manga, V. (2017) Design, synthesis and docking studies of novel 1,2-dihydro-4-hydroxy-2-oxoquinoline-3-carboxamide derivatives as a potential anti-proliferative agents. Eur. J. Med. Chem. 125, 400–410.
4. An, W., Wang, W., Yu, T., Zhang, Y., Miao, Z., Meng, T. and Shen, J. (2016) Discovery of novel 2-phenyl-imidazo[1,2-a]pyridine analogues targeting tubulin polymerization as antiproliferative agents. Eur. J. Med. Chem. 112, 367–372.
5. Romagnoli, R., Baraldi, P. G., Prencipe, F., Oliva, P., Baraldi, S., Salvador, M. K., Lopez-Cara, L. C., Bortolozzi, R., Mattiuzzo, E., Basso, G., et al. (2017) Design, synthesis and biological evaluation of 3-substituted-2-oxindole hybrid derivatives as novel anticancer agents. Eur. J. Med. Chem. 134, 258–270.
6. Xia, Q.H., Hu, W., Li, C., Wu, J.F., Yang, L., Han, X.-M., Shen, Y.-M., Li, Z.-Y. and Li, X. (2016) Design, synthesis, biological evaluation and molecular docking study on peptidomimetic analogues of XK469. Eur. J. Med. Chem. 124, 311–325.
7. Gómez-Jeria, J. S. and Abarca-Martínez, S. (2016) A theoretical approach to the cytotoxicity of a series of β -carboline dithiocarbamate derivatives against prostatic cancer (DU-145), breast cancer (MCF-7), human lung adenocarcinoma (A549) and cervical cancer (HeLa) cell lines. Pharma Chem. 8, 507–526.



8. Gabr, M. T., El-Gohary, N. S., El-Bendary, E. R., El-Kerdawy, M. M. and Ni, N. (2017) Isatin- β -thiocarbohydrazones: Microwave-assisted synthesis, antitumor activity and structure-activity relationship. *Eur. J. Med. Chem.* 128, 36–44.
9. Pogorzelska, A., Sławiński, J., Żołnowska, B., Szafranski, K., Kawiak, A., Chojnacki, J., Ulenberg, S., Zielińska, J. and Bączek, T. (2017) Novel 2-(2-alkylthiobenzenesulfonyl)-3-(phenylprop-2-ynylideneamino)guanidine derivatives as potent anticancer agents – Synthesis, molecular structure, QSAR studies and metabolic stability. *Eur. J. Med. Chem.* 138, 357–370.
10. Gregorić, T., Sedić, M., Grbčić, P., Paravić, A. T., Pavelić, S. K., Cetina, M., Vianello, R. and Raić-Malić, S. (2017) Novel pyrimidine-2,4-dione-1,2,3-triazole and furo[2,3-d]pyrimidine-2-one-1,2,3-triazole hybrids as potential anti-cancer agents: Synthesis, computational and X-ray analysis and biological evaluation. *Eur. J. Med. Chem.* 125, 1247–1267.
11. Gonçalves, B. M. F., Salvador, J. A. R., Marín, S. and Cascante, M. (2016) Synthesis and anticancer activity of novel fluorinated asiatic acid derivatives. *Eur. J. Med. Chem.* 114, 101–117.
12. Cheng, W.-H., Shang, H., Niu, C., Zhang, Z.-H., Zhang, L.-M., Chen, H. and Zou, Z.-M. (2015) Synthesis and Evaluation of New Podophyllotoxin Derivatives with in Vitro Anticancer Activity. *Molecules* 20, 12266–12279.
13. Wu, M., Huang, J., Zhang, J., Benes, C., Jiao, B. and Ren, R. (2017) N-Arachidonoyl Dopamine Inhibits NRAS Neoplastic Transformation by Suppressing Its Plasma Membrane Translocation. *Mol. Cancer Ther.* 16, 57–67.
14. Cheng, W.H., Shang, H., Niu, C., Zhang, Z.H., Zhang, L.-M., Chen, H. and Zou, Z.-M. (2015) Synthesis and Evaluation of New Podophyllotoxin Derivatives with in Vitro Anticancer Activity. *Molecules* 20, 12266–12279.
15. Menicagli, R., Samaritani, S., Signore, G., Vaglini, F. and Dalla Via, L. (2004) In Vitro Cytotoxic Activities of 2-Alkyl-4,6-diheteroalkyl-1,3,5-triazines: New Molecules in Anticancer Research. *J. Med. Chem.* 47, 4649–4652.
16. Ghanbarimasir, Z., Bekhradnia, A., Morteza-Semnani, K., Rafiei, A., Razzaghi-Asl, N. and Kardan, M. (2018) Design, synthesis, biological assessment and molecular docking studies of new 2-aminoimidazole-quinoxaline hybrids as potential anticancer agents. *Spectrochim. Acta. A. Mol. Biomol. Spectrosc.* 194, 21–35.
17. Ghattass, K., El-Sitt, S., Zibara, K., Rayes, S., Haddadin, M. J., El-Sabban, M. and Gali-Muhtasib, H. (2014) The quinoxaline di-N-oxide DCQ blocks breast cancer metastasis in vitro and in vivo by targeting the hypoxia inducible factor-1 pathway. *Mol. Cancer* 13, 12–12.
18. Gu, Z., Li, Y., Ma, S., Li, S., Zhou, G., Ding, S., Zhang, J., Wang, S. and Zhou, C. (2017) Synthesis, cytotoxic evaluation and DNA binding study of 9-fluoro-6H-indolo[2,3-b]quinoxaline derivatives. *RSC Adv.* 7, 41869–41879.
19. Mahapatra, D. K., Bharti, S. K. and Asati, V. (2015) Anti-cancer chalcones: Structural and molecular target perspectives. *Eur. J. Med. Chem.* 98, 69–114.
20. Fytas, C., Zoidis, G., Tsotinis, A., Fytas, G., Khan, M. A., Akhtar, S., Rahman, K. M. and Thurston, D. E. (2015) Novel 1-(2-aryl-2-adamantyl)piperazine derivatives with antiproliferative activity. *Eur. J. Med. Chem.* 93, 281–290.
21. Żołnowska, B., Sławiński, J., Pogorzelska, A., Szafranski, K., Kawiak, A., Stasiłojć, G., Belka, M., Ulenberg, S., Bączek, T. and Chojnacki, J. (2016) Novel 5-Substituted 2-(Aylmethylthio)-4-chloro-N-(5-aryl-1,2,4-triazin-3-yl)benzenesulfonamides: Synthesis, Molecular Structure, Anticancer Activity, Apoptosis-Inducing Activity and Metabolic Stability. *Molecules* 21.
22. Lacroix, M. and Leclercq, G. (2004) Relevance of Breast Cancer Cell Lines as Models for Breast Tumours: An Update. *Breast Cancer Res. Treat.* 83, 249–289.
23. Lozzio, C. and Lozzio, B. (1975) Human chronic myelogenous leukemia cell-line with positive Philadelphia chromosome. *Blood* 45, 321–334.



24. Gao, H., Huang, K.-C., Yamasaki, E. F., Chan, K. K., Chohan, L. and Snapka, R. M. (1999) XK469, a selective topoisomerase II β poison. *Proc. Natl. Acad. Sci.* 96, 12168.
25. Mensah-Osman, E. J., Al-Katib, A. M., Wu, H.-Y., Osman, N. I. and Mohammad, R. M. (2002) 2-[4-(7-Chloro-2-quinoxalinyloxy)phenoxy]-propionic Acid (XK469), an Inhibitor of Topoisomerase (Topo) II β , Up-Regulates Topo II α and Enhances Topo II α -mediated Cytotoxicity 1 The Confocal Imaging Core Facility studies were supported in part by Center Grant P30ES0639 from the National Institute of Environmental Health Sciences and National Cancer Institute Grant P30CA22453. *Mol. Cancer Ther.* 1, 1321.
26. Alousi, A. M., Boinpally, R., Wiegand, R., Parchment, R., Gadgeel, S., Heilbrun, L. K., Wozniak, A. J., DeLuca, P. and LoRusso, P. M. (2007) A phase 1 trial of XK469: Toxicity profile of a selective topoisomerase II β inhibitor. *Invest. New Drugs* 25, 147–154.
27. Ding, Z., Zhou, J.Y., Wei, W.Z., Baker, V. V. and Wu, G. S. (2002) Induction of apoptosis by the new anticancer drug XK469 in human ovarian cancer cell lines. *Oncogene* 21, 4530.
28. Mielcke, T. R., Muradás, T. C., Filippi-Chiela, E. C., Amaral, M. E. A., Kist, L. W., Bogo, M. R., Mascarello, A., Neuenfeldt, P. D., Nunes, R. J. and Campos, M. M. (2017) Mechanisms underlying the antiproliferative effects of a series of quinoxaline-derived chalcones. *Sci. Rep.* 7, 15850.
29. Hong, L., Y, L. X., Balanehru, S., Alexander, N., Fred, V. and D, C. B. Mitotic arrest induced by XK469, a novel antitumor agent, is correlated with the inhibition of cyclin B1 ubiquitination. *Int. J. Cancer* 97, 121–128.
30. Ding, Z., Parchment, R. E., LoRusso, P. M., Zhou, J.-Y., Li, J., Lawrence, T. S., Sun, Y. and Wu, G. S. (2001) The Investigational New Drug XK469 Induces G2-M Cell Cycle Arrest by p53-dependent and -independent Pathways. *Clin. Cancer Res.* 7, 3336–3342.
31. Kessel, D., Reiners, J. J., Hazeldine, S. T., Polin, L. and Horwitz, J. P. (2007) The role of autophagy in the death of L1210 leukemia cells initiated by the new antitumor agents, XK469 and SH80. *Mol. Cancer Ther.* 6, 370.
32. Lin, H., Subramanian, B., Nakeff, A. and Chen, B. D. (2002) XK469, a novel antitumor agent, inhibits signaling by the MEK/MAPK signaling pathway. *Cancer Chemother. Pharmacol.* 49, 281–286.
33. Kpotin, A. G. and Gomez-Jeria, J. S. (2017) A Quantum-chemical Study of the Relationships Between Electronic Structure and Anti-proliferative Activity of Quinoxaline Derivatives on the HeLa Cell Line. *Int. J. Comput. Theor. Chem.* 5, 56–68.
34. Gomez-Jeria, J. S. and Orellana, Í. (2016) A theoretical analysis of the inhibition of the VEGFR-2 vascular endothelial growth factor and the anti-proliferative activity against the HepG2 hepatocellular carcinoma cell line by a series of 1-(4-((2-oxoindolin-3-ylidene)amino)phenyl)-3-aryleureas. *Pharma Chem.* 8, 476–487.
35. Kpotin, A. G., Kankinou, G., Kuevi, U., Gómez Jeria, J. S. and Mensah, J. B. (2017) A Theoretical Study of the Relationships between Electronic Structure and Inhibitory Effects of Caffeine Derivatives on Neoplastic Transformation. *Int. Res. J. Pure Appl. Chem.* 14, 1–10.
36. Gomez-Jeria, J. S. and Valdebenito-Gamboa, J. (2015) A quantum-chemical analysis of the antiproliferative activity of N-3-benzimidazolephenylbisamide derivatives against MGC803, HT29, MKN45 and SW620 cancer cell lines. *Pharma Chem.* 7, 103–121.
37. Robles-Navarro, A. and Gómez Jeria, J. (2016) A quantum-chemical analysis of the relationships between electronic structure and cytotoxicity, GyrB inhibition, DNA supercoiling inhibition and antitubercular activity of a series of quinoline–aminopiperidine hybrid analogues. *Pharma Chem.* 8, 417–440.
38. Gómez-Jeria, J. S. (2017) 45 Years of the KPG Method: A Tribute to Federico Peradejordi. *J. Comput. Methods Mol. Des.* 7, 17–37.
39. Fukui, K. and Fujimoto, H. (1997) Frontier orbitals and reaction paths: selected papers of Kenichi Fukui World Scientific., Fukui Kenichi, Fujimoto Hiroshi, Singapore.



40. Gómez Jeria, J. S. (2013) A new set of local reactivity indices within the Hartree-Fock-Roothaan and density functional theory frameworks. *Can. Chem. Trans.* 1, 25–55.
41. Gomez-Jeria, J. S. and Ojeda-Vergara, M. (2003) Parametrization of the orientational effects in the drug-receptor interaction. *J. Chil. Chem. Soc.* 48, 119–124.
42. Gómez-Jeria, J. S. and Castro-Latorre, P. (2017) A Density Functional Theory analysis of the relationships between the Badger index measuring carcinogenicity and the electronic structure of a series of substituted Benz[a]anthracene derivatives, with a suggestion for a modified carcinogenicity index. *Chem. Res. J.* 2, 112–126.
43. Gómez Jeria, J. S. and Ovando-Guerrero, R. (2017) A DFT Study of the Relationships between Electronic Structure and Central Benzodiazepine Receptor Affinity in a group of Imidazo[1,5-a]quinoline derivatives and a group of 3-Substituted 6-Phenyl-4H-imidazo[1,5-a]-[1,4]benzodiazepines and related compounds. *Chem. Res. J.* 2, 170–181.
44. Bruna-Larenas, T. and Gómez-Jeria, J. S. (2012) A DFT and Semiempirical Model-Based Study of Opioid Receptor Affinity and Selectivity in a Group of Molecules with a Morphine Structural Core. *Int. J. Med. Chem.*
45. Gómez Jeria, J. S. and Surco-Luque, J. C. (2017) A Quantum Chemical Analysis of the Relationships between Electronic Structure and the inhibition of Botulinum Neurotoxin serotype A by a series of Derivatives possessing an 8-hydroxyquinoline core. *Chem. Res. J.* 2, 1–11.
46. Kpotin, A. G., Atohoun, G. S., Kuevi, A. U., Houngue-Kpota, A., Mensah, J.-B. and Gómez Jeria, J. (2016) A quantum-chemical study of the relationships between electronic structure and anti- HIV-1 activity of a series of HEPT derivatives. *J. Chem. Pharm. Res.* 8, 1019–1026.
47. Kpotin, G., Atohoun, S. Y. G., Kuevi, A. U., Kpota-Houngué, A., Mensah, J.-B. and Gómez Jeria, J. S. (2016) A Quantum-Chemical study of the Relationships between Electronic Structure and Trypanocidal Activity against *Trypanosoma Brucei Brucei* of a series of Thiosemicarbazone derivatives. *Pharm. Lett.* 8, 215–222.
48. Gómez-Jeria, J. S. and Moreno-Rojas, C. (2017) Dissecting the drug-receptor interaction with the Klopman-Peradejordi-Gómez (KPG) method. I. The interaction of 2,5-dimethoxyphenethylamines and their N-2-methoxybenzyl-substituted analogs with 5-HT1A serotonin receptors. *Chem. Res. J.* 2, 27–41.
49. Gómez-Jeria, J. S. and Castro-Latorre, P. (2016) On the relationship between electronic structure and carcinogenic activity in substituted Benz[a]anthracene derivatives. *Pharma Chem.* 8, 84–92.
50. Gómez Jeria, J. S. and Flores-Catalán, M. (2013) Quantum-chemical Modeling of the Relationships between Molecular Structure and In Vitro Multi-Step, Multimechanistic Drug Effects. HIV-1 Replication Inhibition and Inhibition of Cell Proliferation as Examples. *Can. Chem. Trans.* 1, 215–237.
51. (2007) G03 Rev. E.01, Gaussian, Pittsburgh, PA, USA.
52. (2014) D-Cent-QSAR: A program to generate Local Atomic Reactivity Indices from Gaussian 03 log files. 1.0, Santiago de Chile.
53. Gómez-Jeria, J. S. (2009) An empirical way to correct some drawbacks of Mulliken Population Analysis (Erratum in: *J. Chil. Chem. Soc.*, 55, 4, IX, 2010). *J. Chil. Chem. Soc.* 54, 482–485.
54. (2015) STERIC: A program for calculating the Orientational Parameters of the substituents 2.0, Santiago de Chile.
55. (1984) Statsoft, Statistica 8.0, 2300 East 14 th St. Tulsa, OK 74104, USA.

